Emergence of a Common Energy Scale Close to the Orbital-Selective Mott Transition

Markus Greger, Marcus Kollar, and Dieter Vollhardt

Theoretical Physics III, Center for Electronic Correlations and Magnetism, Institute of Physics, University of Augsburg, 86135 Augsburg, Germany

(Received 5 June 2012; published 23 January 2013)

We calculate the spectra and spin susceptibilities of a Hubbard model with two bands having different bandwidths but the same on-site interaction, with parameters close to the orbital-selective Mott transition, using dynamical mean-field theory. If the Hund's rule coupling is sufficiently strong, one common energy scale emerges which characterizes both the location of kinks in the self-energy and extrema of the diagonal spin susceptibilities. A physical explanation of this energy scale is derived from a Kondo-type model. We infer that for multiband systems local spin dynamics rather than spectral functions determine the location of kinks in the effective band structure.

DOI: 10.1103/PhysRevLett.110.046403 PACS numbers: 71.27.+a, 71.30.+h

The interactions in correlated metals lead to the emergence of characteristic energy scales. Close to the Fermi energy Landau Fermi-liquid theory [1] applies and the effective electronic dispersion $E_{\boldsymbol{k}}$ is renormalized, but remains linear as in the noninteracting case. The linear dependence terminates at an excitation energy which cannot be calculated within Fermi-liquid theory itself. With increasing strength of the electron-electron interaction, this Fermi-liquid coherence scale decreases and ultimately vanishes at the Mott transition from a metal to an insulator. At the same time charge excitations are shifted to higher energies of the order of the interaction energy and are thus suppressed. For the single-band Hubbard model with on-site Coulomb interaction U, it was shown [2] in dynamical mean-field theory (DMFT) [3] that the Fermi-liquid regime terminates at an energy scale ω_Σ at which the real part of the self-energy, $\mathrm{Re}[\Sigma(\omega)]$, and hence the effective dispersion $E_{\boldsymbol{k}}$, has a rather sudden change in slope [4]. This "kink" does not require any coupling to external bosonic degrees of freedom but is due to the correlated behavior of interacting electrons. For the single-band model the Fermi-liquid scale ω_Σ can be derived from the low-energy properties of the local spectral function [2]. Moreover, it was demonstrated [5,6] that the energy scale ω_Σ is linked to the characteristic energy scale ω_{sp} of spin fluctuations. Kinks in the electronic dispersion were studied theoretically in a variety of contexts [7–15].

In this Letter we explore the origin and characteristic energy scale of kinks in the effective electronic dispersion in a more general context. Employing the DMFT we study a two-band Hubbard model with two different bandwidths W_m, $m = 1, 2$, and the same on-site repulsion U for both bands. The bands are coupled by an interorbital repulsion U_1 and a ferromagnetic Hund's rule spin exchange J. Thereby it is possible to capture orbital effects in correlated materials that do not exist in single-band models. Indeed, different kinks in the dispersion depending on the orbital character are observed for Sr_2RuO_4 both experimentally and theoretically [16,17]. We study the model Hamiltonian

$$\begin{aligned} H &= \sum_{ijm\sigma} t_{ij,m} d^\dagger_{im\sigma} d_{jm\sigma} + H_{\mathrm{int}}, \\ H_{\mathrm{int}} &= U \sum_{im} n_{im\uparrow} n_{im\downarrow} + \sum_{i\sigma\sigma'} (U_1 - \delta_{\sigma\sigma'} J) n_{i1\sigma} n_{i2\sigma'} \\ &\quad + \frac{J}{2} \sum_{im\sigma} d^\dagger_{im\sigma} (d^\dagger_{i\bar{m}\,\bar{\sigma}} d_{im\bar{\sigma}} + d^\dagger_{im\bar{\sigma}} d_{i\bar{m}\,\bar{\sigma}}) d_{i\bar{m}\sigma}, \end{aligned} \tag{1}$$

with spin index $\sigma = \uparrow, \downarrow$ and orbital index $m = 1, 2$. Here a bar over an index denotes the opposite spin or orbital. The two bands do not hybridize but are coupled by the interorbital interactions U_1 and J. We consider U, U_1, and J as independent parameters which can take arbitrary values, but $U_1 = U - 2J$ [18] for d electrons. Half filling ($n = 2$) is assumed throughout. As in the single-band case the correlation strengths of the two bands may be roughly parametrized by the ratios U/W_1 and U/W_2, which are assumed to be unequal. Because of this difference in the relative interaction strengths, an orbital-selective Mott transition (OSMT) occurs upon increase of U [19–36]. We assume semielliptic densities of states, $\rho_m(\epsilon) = (8/\pi)\sqrt{(W_m/2)^2 - \epsilon^2}/W_m^2$, with bandwidths $W_1 < W_2$. Since the hopping amplitudes $t_{ij,m}$ are diagonal in the band index, so are the single-particle Green functions and self-energies. Off-diagonal contributions only occur in two-particle and higher-order correlation functions, e.g., spin and charge susceptibilities.

DMFT can be viewed as the effective theory that results from integrating out all sites except one, which maps a lattice model with local interactions onto an impurity problem in a self-consistently determined host. Thus (1) is mapped onto the following two-impurity Anderson model (TIAM) [29,36]

$$H_{\mathrm{TIAM}} = \sum_{km\sigma} \epsilon_{km} c^{\dagger}_{km\sigma} c_{km\sigma} + \sum_{m\sigma} \epsilon_m n_{m\sigma} + \sum_{km\sigma} (V_{km} c^{\dagger}_{km\sigma} d_{m\sigma} + \mathrm{H.c.}) + H^{\mathrm{loc}}_{\mathrm{int}}, \quad (2)$$

where the local interaction $H^{\mathrm{loc}}_{\mathrm{int}}$ has the same form as H_{int}, but without the index i. The DMFT self-consistency conditions demand that the band energies ϵ_{km} and hybridizations V_{km} are determined such that Green functions and self-energies of (2) equal the corresponding local lattice quantities,

$$G_m(\omega) = \int d\epsilon \frac{\rho_m(\epsilon)}{\omega + i0 - \epsilon_m - \Sigma_m(\omega) - \epsilon}, \quad (3a)$$

$$\Sigma_{m\sigma}(\omega) = \omega + i0 - \epsilon_m - \frac{1}{G_m(\omega)} - \Delta_m(\omega), \quad (3b)$$

which take the same form as for two decoupled one-band models due to the absence of interorbital hopping. Here the hybridization function is defined as $\Delta_m(\omega) = \sum_{\boldsymbol{k}} |V_{\boldsymbol{k}m}|^2/(\omega + i0 - \epsilon_{\boldsymbol{k}m})$. We solve the impurity model using the numerical renormalization group, which allows us to obtain previously inaccessible dynamical quantities at zero temperature on the real frequency axis (see Supplemental Material [37]). With this we compute the spectral functions $A_m(\omega) = -\mathrm{Im}[G_m(\omega)]/\pi$, self-energies $\Sigma_m(\omega)$, and spin susceptibilities $\chi^{\mathrm{sp}}_m(\omega) = (-1/\pi)\mathrm{Im}\langle\langle S^z_m; S^z_m\rangle\rangle_\omega$ for the two bands in the metallic phase close to the OSMT and monitor the behavior as a function of the Hund's rule coupling J. The different correlation strengths of the orbitals lead to different behavior of the spectral functions and self-energies which are shown in Figs. 1 and 2. The overall behavior corresponds to that of two Fermi liquids with different mass renormalizations, reminiscent of two uncoupled one-band Hubbard models with different local interactions. In all cases the single-particle spectra $A_1(\omega)$ and $A_2(\omega)$ differ significantly, especially close to the OSMT when the spectral function of the narrow band has a very sharp central peak. Because the spectrum of each band depends mostly on the correlation strength U/W_m but not much on Hund's rule exchange J, the latter was previously characterized as a "band decoupler" [27], at least for the charge degrees of freedom, in the sense that the spectrum of each of the bands tends to be similar to the single-band case. Quantum Monte Carlo results [22,24,26,29,33] suggest that at $T = 0$ the low-frequency behavior of $\mathrm{Re}[\Sigma_m]$ and χ^{sp}_m is then also different. Figure 1 shows that this is indeed the case, but only for $J = 0$ and $U_1 \neq 0$.

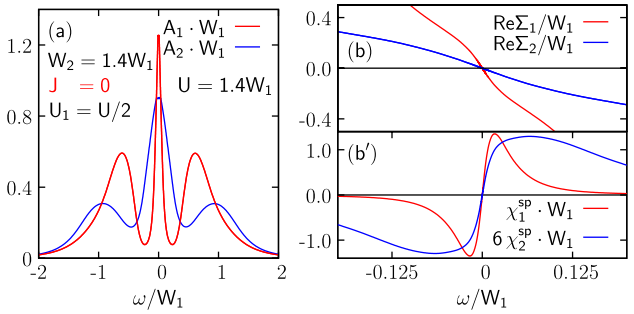

FIG. 1 (color online). For $J = 0$ and $U_1 \neq 0$ the difference in the correlation strength of the two bands is observed not only in the shape of the spectral function $A_m(\omega)$ (a), but also in the corresponding band-resolved self-energies and spin susceptibilities (b), (b′).

Indeed, a finite Hund's rule coupling leads to a fundamentally different low-energy behavior of $\mathrm{Re}[\Sigma_m]$ and χ^{sp}_m. Namely, as the system approaches the OSMT we find that at low energies these quantities become proportional, i.e., $\mathrm{Re}[\Sigma_1(\omega)] \propto \mathrm{Re}[\Sigma_2(\omega)]$ and $\chi^{\mathrm{sp}}_1(\omega) \propto \chi^{\mathrm{sp}}_2(\omega)$; the consequences for other dynamical quantities are discussed in the Supplemental Material [37]. As illustrated in Figs. 2(b), 2(b′), 2(d), and 2(d′), this striking result cannot be inferred from the spectral functions $A_m(\omega)$ since the shape and the characteristic energy scales of the latter differ considerably and thus suggest a decoupled behavior. The characteristic energy scale of the spin fluctuations is given by the locations ω^{sp}_m of the extrema in the spin susceptibilities $\chi^{\mathrm{sp}}_m(\omega)$. The proportionalities discussed above imply that the system has identical spin fluctuation energy scales ($\omega^{\mathrm{sp}}_1 = \omega^{\mathrm{sp}}_2$), Fermi-liquid energy scales, and kinks ($\omega^{\Sigma}_1 = \omega^{\Sigma}_2$), *irrespective* of the different correlation strengths of the bands. Furthermore, the self-energy kinks and the strongest spin fluctuations occur at the same energy

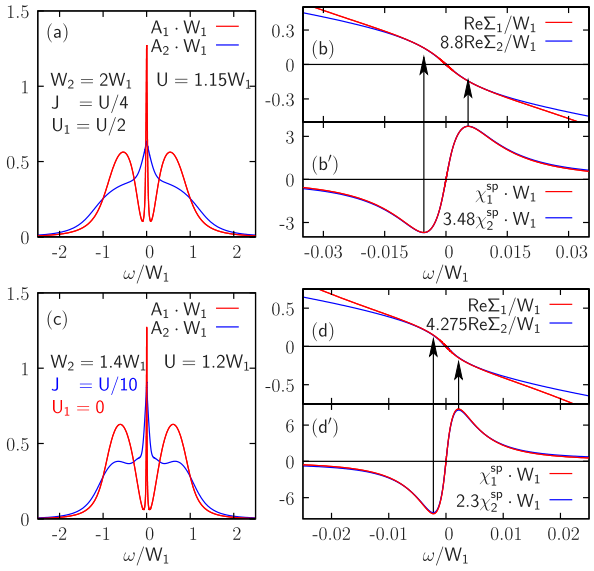

FIG. 2 (color online). In the metallic phase close to the OSMT a striking proportionality, $\mathrm{Re}[\Sigma_1] \propto \mathrm{Re}[\Sigma_2]$ and $\chi^{\mathrm{sp}}_1 \propto \chi^{\mathrm{sp}}_2$ [(b), (b′), (d), (d′)] is seen to emerge for $J > 0$, which is in marked contrast to the decoupled behavior in Fig. 1. Very close to the OSMT (d), (d′) even a weak exchange coupling J leads to a common low-energy scale. Note that U_1 has little influence on the qualitative low-energy behavior. The system enters the OSMT phase for $U \lesssim 1.3W_1$ (a) and $U < 1.25W_1$ (c).

in each band, $\omega_m^\Sigma \simeq \omega_m^{sp}$ (as observed also in the single-band case [5]), which means that for the two-band model (1) a single common low-energy scale emerges for kinks and spin fluctuations in both bands. For our numerical data we define the kink scale ω_m^Σ as the energy for which the extrapolated linear dispersion near the Fermi energy deviates from $\mathrm{Re}[\Sigma_m(\omega)]$ by 20%, which agrees well with the perceived location of the kinks in Figs. 2(b) and 2(d). The corresponding momentum-resolved spectral function $A_{\boldsymbol{k}}(\omega)$ and effective dispersions $E_{\boldsymbol{k}m}$ are shown in Fig. 3. We observe that although the slope of the Fermi-liquid dispersion is very different for the two bands, the linear regimes terminate at the *same* energy scale, which, however, slightly deviates from ω_m^Σ due to band structure effects.

By comparing the results for $J = 0$ in Fig. 1 with $J \neq 0$ in Figs. 2(b), 2(b′), and 2(c), it is clear that U_1 cannot be responsible for the common energy scale. This effect only appears in the presence of the Hund's rule coupling J, whereas U_1 merely leads to quantitative modifications. We will therefore consider only $U_1 = 0$ in the following in order to better resolve the effect of the Hund's rule coupling J. (Additional data for $U_1 = U - 2J$ are provided in the Supplemental Material [37].) Starting from $J = 0$ we study the continuous evolution of the two initially uncoupled Hubbard models into the "locked" regime. To this end we obtain spin fluctuation scales $\omega_m^{sp}(J)$ and self-energy kinks $\omega_m^\Sigma(J)$ for the two orbitals for two different values of U/W_1 [Figs. 4(a) and 4(b)]. As J is increased, both orbital-resolved energy scales approach each other and finally merge into a single scale, as seen in Figs. 2(c), 2(d), and 2(d′). Comparing Figs. 4(a) and 4(b), we observe that this common low-energy scale appears at a threshold value which decreases for increasing U. We also notice the very close correspondence between kink energies and spin fluctuation scales, especially in the more strongly correlated case [Fig. 4(b)]. This observation can be understood in terms of local Fermi-liquid theory [38]: similarly to the single-band case [5,6], the linear regime in $\mathrm{Re}\Sigma(\omega)$ must terminate at the frequency $\omega_m^\Sigma \simeq \omega_m^{sp}$, when the spin fluctuations become strong enough to destroy the local Fermi liquid. As expected, the kink energy scale derived in Ref. [2], $\omega_m^\star = 0.2 Z_m W_m$, applies only to the narrow band with its well-developed three-peak spectral function and not to the wide band [cf. solid and dashed lines in Fig. 4(b) corresponding to $0.8\omega_m^\star$ [39]].

In the vicinity of the OSMT the characteristic energies $\omega_m^{sp}(J)$ and $\omega_m^\Sigma(J)$ represent equivalent energy scales. It thus suffices to discuss the J dependence of $\omega_m^{sp}(J)$ in the following. To explain the locking of the low-energy scales for the two bands we proceed in two steps; see Figs. 4(c) and 4(d).

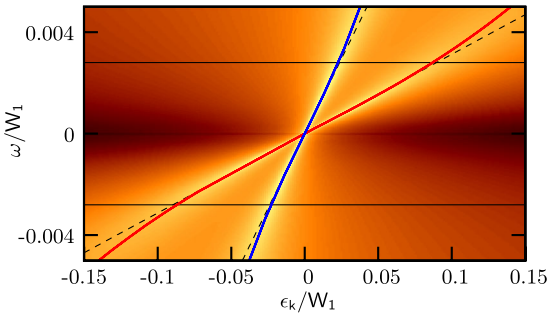

FIG. 3 (color online). Intensity plot of the total spectral density $A_{\boldsymbol{k}}(\omega)$ deep inside the central peaks as a function of $\epsilon_{\boldsymbol{k}}$ and ω [parameters as in Figs. 2(a) and 2(b)]. The effective dispersion $E_{\boldsymbol{k},m}$ is defined by its local maxima [light gray (blue) or dark gray (red) line for the wide or narrow band]. It is linear (dashed lines) in the Fermi-liquid regime close to the Fermi surface and has kinks at the same energy $\sim \pm 0.0028 W_1$ for both bands (horizontal lines).

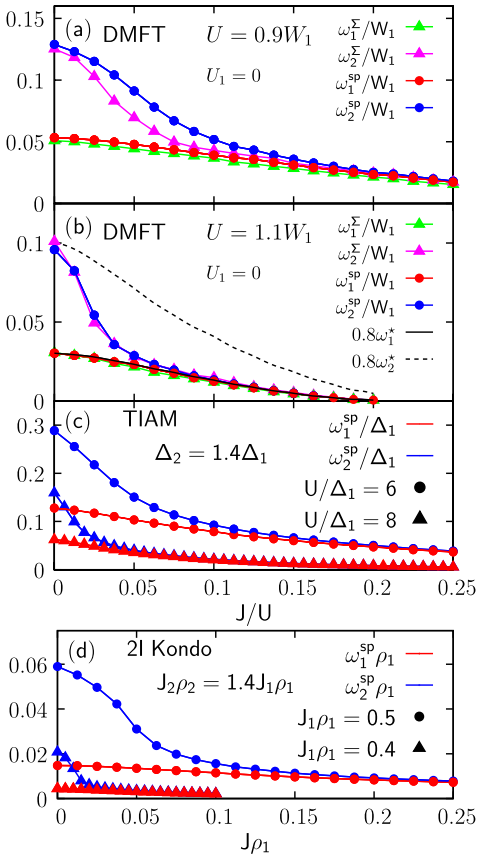

FIG. 4 (color online). (a), (b) Orbitally resolved kink energies $\omega_{1,2}^\Sigma(J)$ and extrema $\omega_{1,2}^{sp}(J)$ of the spin susceptibilities as calculated within DMFT for different Hubbard interactions U. Sufficiently large U leads to $\omega_m^\Sigma(J) = \omega_m^{sp}(J)$ and sufficiently large J leads to $\omega_1^\Sigma(J) = \omega_2^\Sigma(J)$ and $\omega_1^{sp}(J) = \omega_2^{sp}(J)$. The dashed lines in (b) mark the single-band estimates for ω_m^Σ [2] which match well for the narrow but not the wide band (see text). (c) A simplified Anderson impurity model and (d) a related two-impurity Kondo model, both with a behavior similar to the DMFT solution. Note that the system in (b) enters the OSMT phase at approximately $J = 0.2U$; in (a) the transition occurs for unrealistically high values $J \gtrsim 1.1U$.

First we establish that the locking is an intrinsic property of the underlying TIAM Hamiltonian and is only quantitatively modified by the DMFT self-consistency equations (3). Then we compare with the results for a Kondo-type model that allows us to identify the competing couplings and elementary excitations. For the first step we solve the impurity model (2) with different but *constant* hybridization functions $[\Delta_2(\omega) = 1.4\Delta_1(\omega) = \text{const}]$ and extract $\omega_m^{\text{sp}}(J)$ from $\chi_1^{\text{sp}}(\omega)$. The result is depicted in Fig. 4(c) for two values of U, showing very good qualitative agreement with the DMFT results in Figs. 4(a) and 4(b). In particular, the common low-energy scale emerges at a value of J which decreases with increasing U in a similar fashion. We conclude that the DMFT self-consistency induces only minor modifications as long as the system remains in the metallic phase.

In a second step we focus on the low-energy spin dynamics close to the OSMT. In this regime charge excitations are strongly suppressed. This limit of (2) is described by the following two-impurity Kondo model (2IKM) [40–42],

$$H_{\text{2IKM}} = \sum_{\boldsymbol{k}m\sigma} \epsilon_{\boldsymbol{k}m} c^\dagger_{\boldsymbol{k}m\sigma} c_{\boldsymbol{k}m\sigma} + \sum_m J_m \boldsymbol{s}_m \cdot \boldsymbol{S}_m - J \boldsymbol{S}_1 \cdot \boldsymbol{S}_2, \quad (4)$$

where $\boldsymbol{S}_m$ are the impurity spin operators. The antiferromagnetic couplings J_m stem from superexchange processes and decrease with increasing U while $J > 0$ is the Hund's exchange interaction of (2). Thus (4) also represents the low-energy sector of (1), but with J_m determined by the DMFT self-consistency equations. We take $J_2\rho_2(0) = 1.4J_1\rho_1(0)$, starting from $\omega_1^{\text{sp}}(0) \neq \omega_2^{\text{sp}}(0)$ for $J = 0$. The J dependence of $\omega_m^{\text{sp}}(J)$ is shown in Fig. 4(d). The qualitative agreement among the results obtained for all three models (DMFT, TIAM with constant hybridization, 2IKM) confirms that Eq. (4) already describes the essential processes that lead to the emergence of the joint low-energy scale. In the 2IKM the spins will align for low-excitation energies and form a composite spin-1 state [40]. This happens roughly when the energy gain $\omega_1^{\text{sp}}(J) + \omega_2^{\text{sp}}(J)$ due to Kondo screening of the two impurities is overcome by $J/4$, the approximate energy gain due to the ferromagnetic exchange. Hence the locking of the low-energy scales sets in at about $J \approx \omega_m^{\text{sp}}(J)/8$, as seen in Figs. 4(a) ($J \approx 0.2W_1$) and 4(b) ($J \approx 0.1W_1$). We conclude that two impurity spins exhibit joint low-energy fluctuations and hence proportional χ_m^{sp}'s if J dominates over the individual spin fluctuation scales ω_m^{sp} and are essentially independent otherwise. Regarding the influence of U, we note that the antiferromagnetic couplings between the spins and the baths decrease with increasing interaction; i.e., more correlated systems exhibit stronger locking of their spins and their low-energy scales. Thus, J couples the low-energy scales more effectively for stronger correlations, as seen in Figs. 4(a)–4(c). Thus, any nonzero $J > 0$ will lead to this locking as U approaches the OSMT, as then J_1 vanishes in (4). We note that for this mechanism the ratio W_2/W_1 of bandwidths and the value of the density interaction U_1 play only a minor role (see further data in the Supplemental Material [37]).

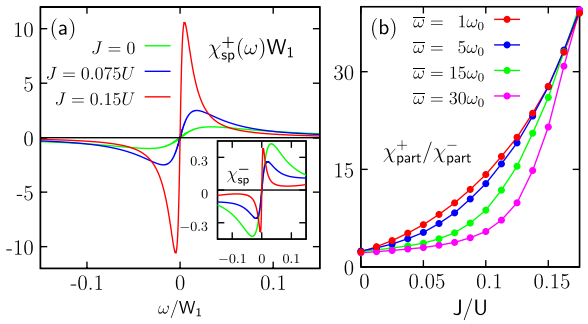

FIG. 5 (color online). The correlation functions $\chi^+_{\text{sp}}(\omega)$ and $\chi^-_{\text{sp}}(\omega)$ indicate the creation of a composite spin-1 state for large J [light gray (green) curves in (a) and in the inset have about the same magnitude; also note the different scales in (a) and the inset]. Accordingly, the partial spectral weight fraction $\chi^+_{\text{part}}/\chi^-_{\text{part}}$ in (b) grows strongly with J and is only quantitatively affected by the upper limit $\bar{\omega}$. Here, $\omega_0 = \max[\omega_1^{\text{sp}}(J), \omega_2^{\text{sp}}(J)]$.

To explicitly verify the physical picture described above, we investigate the correlation functions

$$\chi^{\pm}_{\text{sp}}(\omega) = -\frac{1}{\pi} \text{Im}\langle\langle S_1^z \pm S_2^z | S_1^z \pm S_2^z \rangle\rangle_\omega \quad (5)$$

in DMFT. They describe the dynamics of the composite local triplet $[\chi^+(\omega)]$ and the "residual" singlet $[\chi^-(\omega)]$, respectively, and are plotted in Fig. 5(a). As expected, for both susceptibilities the positions of their maxima decreases with increasing interaction. However, only the triplet susceptibility shows a resonance that also increases in amplitude. In Fig. 5(b) we plot the weight $\chi^{\pm}_{\text{part}} = \int_0^{\bar{\omega}} \chi^{\pm}(\omega) d\omega$ as a function of J for several values of the cutoff $\bar{\omega}$. Especially for larger values of J the residual spin contributes only little to the total low-energy spin response $\chi_1^{\text{sp}} + \chi_2^{\text{sp}}$ of the system, which is thus well described by $\chi^+(\omega)$. This establishes the formation of the composite spin-1 state as the physical origin for the emergence of the common energy scale. Namely, as the OSMT is approached by increasing U, the antiferromagnetic superexchange of the narrow and wide band both decrease until J becomes the dominating scale, at least for the spins in the narrow band. The spins align and exhibit joint low-energy dynamics, leading to the proportionalities of $\text{Re}[\Sigma_m(\omega)]$ and $\chi_m^{\text{sp}}(\omega)$ for the two bands. We note that for this mechanism the ratio W_2/W_1 of bandwidths and the value of U_1 play only a minor role (see Supplemental Material [37] for further data for other parameter values).

In summary, we showed that the physical picture developed previously for single-band systems close to the Mott transition is significantly modified for a two-band model with Hund's rule coupling, due to the formation of a local spin-1 state. As a consequence, a common low-energy scale emerges for the two bands at which kinks in the

self-energies and maxima of the spin susceptibilities appear. Moreover, these quantities for the two bands are proportional to each other over a wide frequency range. In practice, if the angle-resolved photoemission spectroscopy spectrum of a correlated material exhibits kinks at the same binding energy in bands with different correlation strengths (as in Fig. 3), this may indicate that J is sufficiently large to lock these energy scales and the system is close to an OSMT.

We thank R. Žitko for releasing his NRG code, on which our code is based [43], and L. Chioncel and J. Otsuki for useful discussions. This work was supported by the Deutsche Forschungsgemeinschaft through TRR 80.

[1] D. Pines and P. Nozières, *The Theory of Quantum Liquids* (Benjamin, New York, 1966), Vol. I.
[2] K. Byczuk, M. Kollar, K. Held, Y.-F. Yang, I. A. Nekrasov, T. Pruschke, and D. Vollhardt, Nat. Phys. **3**, 168 (2007).
[3] W. Metzner and D. Vollhardt, Phys. Rev. Lett. **62**, 324 (1989); A. Georges, G. Kotliar, W. Krauth, and M. J. Rozenberg, Rev. Mod. Phys. **68**, 13 (1996); G. Kotliar and D. Vollhardt, Phys. Today **57**, No. 3, 53 (2004).
[4] An effective dispersion E_k can always be defined by the maxima of the momentum-resolved spectral function $A_k(\omega)$, which is essentially measured in angular-resolved photoemission spectroscopy, even when the spectrum is rather incoherent and no sharp quasiparticle excitations occur.
[5] C. Raas, P. Grete, and G. S. Uhrig, Phys. Rev. Lett. **102**, 076406 (2009).
[6] P. Grete, S. Schmitt, C. Raas, F. B. Anders, and G. S. Uhrig, Phys. Rev. B **84**, 205104 (2011).
[7] M. Eschrig and M. R. Norman, Phys. Rev. Lett. **85**, 3261 (2000).
[8] D. Manske, I. Eremin, and K. H. Bennemann, Phys. Rev. Lett. **87**, 177005 (2001).
[9] Y. Kakehashi and P. Fulde, J. Phys. Soc. Jpn. **74**, 2397 (2005).
[10] I. A. Nekrasov, K. Held, G. Keller, D. E. Kondakov, T. Pruschke, M. Kollar, O. K. Andersen, V. I. Anisimov, and D. Vollhardt, Phys. Rev. B **73**, 155112 (2006).
[11] A. Toschi, M. Capone, C. Castellani, and K. Held, Phys. Rev. Lett. **102**, 076402 (2009).
[12] A. Hofmann, X. Y. Cui, J. Schäfer, S. Meyer, P. Höpfner, C. Blumenstein, M. Paul, L. Patthey, E. Rotenberg, J. Bünemann, F. Gebhard, T. Ohm, W. Weber, and R. Claessen, Phys. Rev. Lett. **102**, 187204 (2009).
[13] X. Deng, M. Ferrero, J. Mravlje, M. Aichhorn, and A. Georges, Phys. Rev. B **85**, 125137 (2012).
[14] J. Bauer and G. Sangiovanni, Phys. Rev. B **82**, 184535 (2010).
[15] A. Kainz, A. Toschi, R. Peters, and K. Held, Phys. Rev. B **86**, 195119 (2012).
[16] H. Iwasawa, Y. Aiura, T. Saitoh, I. Hase, S. I. Ikeda, Y. Yoshida, H. Bando, M. Higashiguchi, Y. Miura, X. Y. Cui, K. Shimada, H. Namatame, and M. Taniguchi, Phys. Rev. B **72**, 104514 (2005).
[17] J. Mravlje, M. Aichhorn, T. Miyake, K. Haule, G. Kotliar, and A. Georges, Phys. Rev. Lett. **106**, 096401 (2011).
[18] C. Lyon-Caen and M. Cyrot, J. Phys. C **8**, 2091 (1975).
[19] V. I. Anisimov, I. A. Nekrasov, D. E. Kondakov, T. M. Rice, and M. Sigrist, Eur. Phys. J. B **25**, 191 (2002).
[20] T. Pruschke and R. Bulla, Eur. Phys. J. B **44**, 217 (2005).
[21] A. Liebsch, Phys. Rev. Lett. **95**, 116402 (2005); T. A. Costi and A. Liebsch, Phys. Rev. Lett. **99**, 236404 (2007).
[22] C. Knecht, N. Blümer, and P. G. J. van Dongen, Phys. Rev. B **72**, 081103 (2005).
[23] E. Jakobi, N. Blümer, and P. G. J. van Dongen, Phys. Rev. B **80**, 115109 (2009).
[24] R. Arita and K. Held, Phys. Rev. B **72**, 201102 (2005).
[25] S. Biermann, L. de'Medici, and A. Georges, Phys. Rev. Lett. **95**, 206401 (2005).
[26] L. de'Medici, A. Georges, and S. Biermann, Phys. Rev. B **72**, 205124 (2005).
[27] L. de'Medici, Phys. Rev. B **83**, 205112 (2011).
[28] A. Koga, N. Kawakami, T. M. Rice, and M. Sigrist, Phys. Rev. Lett. **92**, 216402 (2004); K. Inaba, A. Koga, S. I. Suga, and N. Kawakami, Phys. Rev. B **72**, 085112 (2005).
[29] A. Koga, N. Kawakami, T. Rice, and M. Sigrist, Physica (Amsterdam) **359–361B**, 1366 (2005).
[30] P. Werner and A. J. Millis, Phys. Rev. B **74**, 155107 (2006).
[31] J. Bünemann, D. Rasch, and F. Gebhard, J. Phys. Condens. Matter **19**, 436 206 (2007).
[32] K. Inaba and A. Koga, J. Phys. Soc. Jpn. **76**, 094712 (2007).
[33] K. Bouadim, G. G. Batrouni, and R. T. Scalettar, Phys. Rev. Lett. **102**, 226402 (2009).
[34] R. Peters and T. Pruschke, Phys. Rev. B **81**, 035112 (2010).
[35] W.-C. Lee and P. W. Phillips, Phys. Rev. B **84**, 115101 (2011).
[36] L. de'Medici, J. Mravlje, and A. Georges, Phys. Rev. Lett. **107**, 256401 (2011); A. Georges, Ann. Phys. (Berlin) **523**, 672 (2011); K. Inaba and A. Koga, Phys. Rev. B **73**, 155106 (2006).
[37] See Supplemental Material at http://link.aps.org/supplemental/10.1103/PhysRevLett.110.046403 for further calculations and details regarding the numerical method.
[38] P. Nozières, J. Low Temp. Phys. **17**, 31 (1974).
[39] The prefactor of 0.8 accounts for our present kink criterion (20% deviation of $\mathrm{Re}\Sigma_m$ from the linear extrapolation), which differs slightly from that in Ref. [2].
[40] C. Jayaprakash, H. R. Krishna-murthy, and J. W. Wilkins, Phys. Rev. Lett. **47**, 737 (1981).
[41] B. A. Jones and C. M. Varma, Phys. Rev. Lett. **58**, 843 (1987).
[42] S. Yotsuhashi, H. Kusunose, and K. Miyake, J. Phys. Soc. Jpn. **70**, 186 (2001).
[43] R. Žitko, Comput. Phys. Commun. **182**, 2259 (2011); http://nrgljubljana.ijs.si.